JACS JOURNAL OF THE AMERICAN CHEMICAL SOCIETY

Article

Cite This: J. Am. Chem. Soc. 2018, 140, 17724−17733

pubs.acs.org/JACS

Supramolecular Packing and Macroscopic Alignment Controls Actuation Speed in Macroscopic Strings of Molecular Motor Amphiphiles

Franco King-Chi Leung,[†] Tobias van den Enk,[†] Takashi Kajitani,[‡,§] Jiawen Chen,[†] Marc C. A. Stuart,[†] Jeroen Kuipers,[∥] Takanori Fukushima,[‡] and Ben L. Feringa*[,†]

[†]Center for System Chemistry, Stratingh Institute for Chemistry, University of Groningen, Nijenborgh 4, 9747 AG Groningen, The Netherlands

[‡]Laboratory for Chemistry and Life Science, Institute of Innovative Research, Tokyo Institute of Technology, 4259 Nagatsuta, Midori-ku, Yokohama 226-8503, Japan

[§]RIKEN SPring-8 Center, 1-1-1 Kouto, Sayo, Hyogo 679-5148, Japan

[∥]Department of Cell Biology, Molecular Imaging and Electron Microscopy, University Medical Center Groningen, University of Groningen, 9712 CP Groningen, The Netherlands

Supporting Information

ABSTRACT: Three-dimensional organized unidirectionally aligned and responsive supramolecular structures have much potential in adaptive materials ranging from biomedical components to soft actuator systems. However, to control the supramolecular structure of these stimuli responsive, for example photoactive, materials and control their actuation remains a major challenge. Toward the design of "artificial muscles", herein, we demonstrate an approach that allows hierarchical control of the supramolecular structure, and as a consequence its photoactuation function, by electrostatic interaction between motor amphiphiles (MA) and counterions. Detailed insight into the effect of various ions on structural parameters for self-assembly from nano- to micrometer scale in water including nanofiber formation and nanofiber aggregation as well as the packing structure, degree of alignment, and actuation speed of the macroscopic MA strings prepared from various metal chlorides solution, as determined by electronic microscopy, X-ray diffraction, and actuation speed measurements, is presented. Macroscopic MA strings prepared from calcium and magnesium ions provide a high degree of alignment and fast response photoactuation. By the selection of metal ions and chain length of MAs, the macroscopic MA string structure and function can be controlled, demonstrating the potential of generating multiple photoresponsive supramolecular systems from an identical molecular structure.

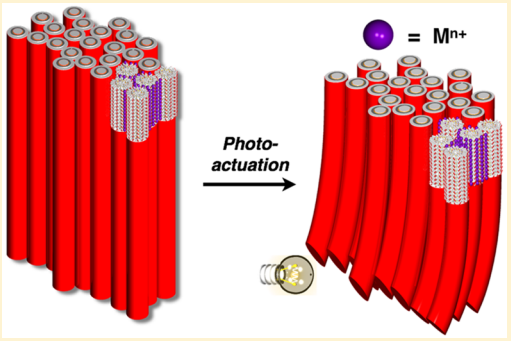

INTRODUCTION

Supramolecular polymers are found in many living systems, for example, cytoskeleton filaments (F-actin[1] and microtubules[2]), flagellar filaments of bacteria,[3] and polymers of viral proteins and muscles,[4] to serve vital roles in key biological functions. While biological systems provide precise control in supramolecular polymerization,[1−4] synthetic supramolecular polymers[5,6,14] in aqueous media allow tunable features due to the design based on synthetic compounds and bioinspired functionality.[6,7,16,17,8−15] This delicate molecular design strategy allows the construction of hierarchical supramolecular assemblies along multiple-length-scales. At the microscopic length-scale level,[10,11] numerous unimolecular amphiphilic molecules have been shown to assemble into highly ordered one-dimensional (1D) supramolecular systems, through noncovalent interaction, for example, hydrogen bonding,[18−25] arene interaction,[26−33] and electrostatic effects.[32,34−37] At macroscopic length-scales, the obtained 1D supramolecular polymers of unimolecular amphiphiles can further assemble, instead of forming a three-dimensional (3D) randomly entangled network, into 3D unidirectionally aligned hierarchical supramolecular structures, providing exciting opportunities toward applications for instance in regenerative (biomedical) materials,[38−40] actuators, electronics, and optoelectronic materials.[41−43] To further demonstrate the importance of 3D unidirectionally aligned hierarchical supramolecular structures, we recently reported that a photoresponsive hierarchical supramolecular assembled structure derived from an amphiphilic molecular motor with precise control of molecular organization and cooperativity allows energy conversion, accumulation of strain, and amplification of the molecular

Received: October 6, 2018
Published: November 21, 2018

DOI: 10.1021/jacs.8b10778
J. Am. Chem. Soc. 2018, 140, 17724−17733

rotation of motor amphiphile (MA) to macroscopic muscle-like contractive motions.[44] This supramolecular approach provides a complementary method to the existing macroscopic actuators obtained by stimuli-responsive crystals,[45−48] polymeric gels,[49−52] and polymeric liquid crystals.[53−59]

The dynamic nature of the supramolecular polymers provides inherent sensitivity of the assembled structure to the external environment, for example, chemicals, solvents, external shear force, electric and magnetic fields. In addition, the design of molecular amphiphiles allows precise control over the hierarchical structure from microscopic to macroscopic length-scale and their intrinsic functions.[34,44] Notably, electrostatic screening of amphiphilic self-assembled structures, pioneered by Stupp et al., by careful choice of counterions, provides a mean to control stiffness of 3D randomly entangled supramolecular structures[60−62] and has enabled to govern important functions, for example, cell proliferation, differentiation, adhesion, and migration.[63−65] However, the control of 3D unidirectionally aligned hierarchical supramolecular structure by a single non-invasive external stimulus, without covalent chemical modification of the molecular amphiphiles structure, at different length-scale and as a consequence its function remains highly challenging.

In our recently reported artificial muscle, the electrostatic interaction between carboxylate groups of MA and Ca^{2+} allows the MA nanofiber stabilization and the formation of a MA macroscopic string using a shear flow method to provide unidirectionally aligned MA strings for photoactuation. We envisioned that by manipulating the electrostatic interaction of the carboxylate groups of MA and its counter-cations (M^{n+}) allows further control of the hierarchical assembled structure of the motor amphiphile and elucidates key parameters for supramolecular aggregation (Figure 1). The nature of the cationic counterion effect on the organization of MA might enable the control of induction of nanofibers formation, aggregation of nanofibers, structural order parameters of the unidirectionally aligned structures, and speed of photoactuation of the string of unidirectionally aligned nanofibers. Additionally, the side chains of MA are modified to provide insight in the effect of the chain length effect on the structure and functioning of MA macroscopic strings. By elucidating the key design of supramolecular muscles, ultimately, this could open up new prospects toward the development of controllable stimuli-responsive materials and future soft robotic systems.

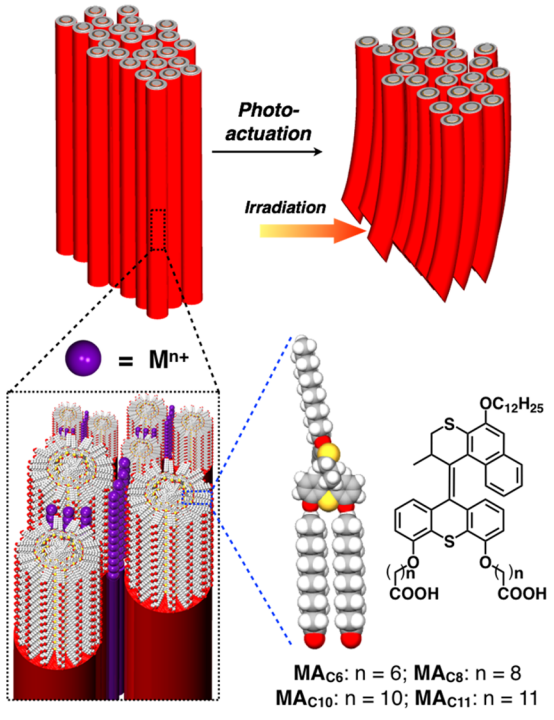

Figure 1. Molecular structures of molecular motor amphiphiles and the hierarchical organization and photoactuation process of their assembled structures in the macroscopic string.

RESULTS AND DISCUSSION

Molecular Design and Synthesis. The motor amphiphile was designed with a second-generation molecular motor core, and a dodecyl chain was attached to the upper half, and two carboxyl groups connected with alkyl-linkers to the lower half (Figure 1). In addition to the countercation effect, we envision that various chain lengths of the alkyl-linker, which connected the two carboxyl groups to the lower half of the motor unit, allow for systematic modification of the packing in the resultant MA string and its actuation function. Motor amphiphiles with shorter chain lengths, $\mathbf{MA}_{C6}$ and $\mathbf{MA}_{C8}$, as well as longer chain lengths, $\mathbf{MA}_{C11}$, were designed (Figure 1). The general synthesis is summarized in Scheme 1. Compounds **1** and **4** were prepared by our reported procedures[44] (Scheme 1). The key step in the synthesis of $\mathbf{MA}_{C6}$, $\mathbf{MA}_{C8}$, and $\mathbf{MA}_{C11}$ is the formation of the central overcrowded olefinic bond by

Scheme 1. Synthesis of Motor Amphiphiles[a]

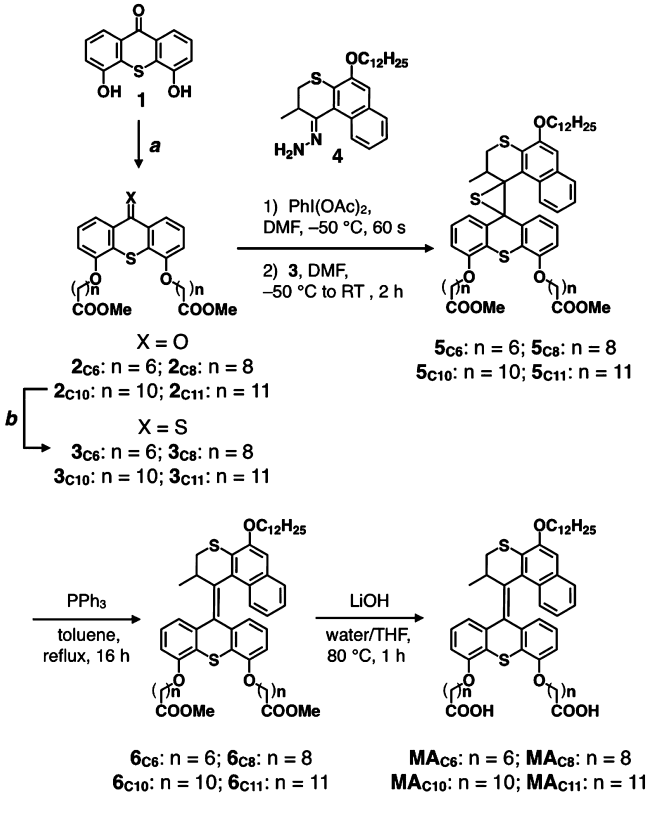

[a]Reagents and conditions: (a) $BrC_6H_{12}COOMe$, $BrC_8H_{16}COOMe$, $BrC_{10}H_{20}COOMe$, or $BrC_{11}H_{22}COOMe$, K_2CO_3, DMF, 85 °C, 16 h; (b) Lawesson's reagent, toluene, 100 °C, 1 h. Yields and detailed procedures are provided in Supporting Information.

DOI: 10.1021/jacs.8b10778
J. Am. Chem. Soc. 2018, 140, 17724−17733

diazo-thioketone coupling (Scheme 1). The precursors **2** were obtained by Williamson ether formation of thioxanthone **1** with the corresponding alkyl bromides in the presence of K_2CO_3 in DMF, followed by conversion into the corresponding thioketones **3** with Lawesson's reagents in toluene. Hydrazone **4** was *in situ* oxidized with diacetoiodobenzene in DMF into the corresponding diazo compound, and subsequent addition of the freshly prepared thioketones **3** provided the corresponding episulfides **5**. Desulfurization with triphenylphosphine in toluene gave the corresponding overcrowded alkenes **6**. The motor amphiphiles **MAs** were obtained by hydrolysis of the ester groups into carboxylic acid groups in the presence of LiOH in water and THF. The structures of all new motor amphiphiles were unambiguously determined by ^{1}H, ^{13}C NMR, and high-resolution ESI-TOF mass spectrometry (Figures S15−S37).

Ionic Effect of MA_{C10} Assembled Structure. Freshly prepared aqueous solutions of $\mathbf{MA_{C10}}$ with 2 equiv of sodium hydroxide were heated at 80 °C for 30 min and cooled down to room temperature to afford a colorless transparent solution, indicating that the deprotonated form is soluble up to 50.0 mM concentration. A Nile Red fluorescence assay (NRFA), which probes the internal hydrophobicity of assemblies,[66] revealed a decrease in blue shift when diluting beyond 0.01 mM and showed a critical aggregation concentration (CAC) of 2.67 μM (Figure 2a). The $\mathbf{MA_{C10}}$ assemblies formed by the water-soluble carboxylates were imaged using cryogenic transmission electron microscopy (cryo-TEM) to capture their solution-state morphologies. $\mathbf{MA_{C10}}$ assembled into fibers hundreds of nanometers to micrometers in length at 5.0 mM concentration (Figure S1a), while no nanostructure was observed below CAC (Figure S1b). To investigate the countercation effect of LiCl, NaCl, KCl, $BeCl_2$, $MgCl_2$, $CaCl_2$, $SrCl_2$, $BaCl_2$, and $ScCl_3$ on nanofiber formation of the $\mathbf{MA_{C10}}$, NRFA was employed to probe the change of internal hydrophobicity of the $\mathbf{MA_{C10}}$ assembly. The blue shift of Nile Red was monitored in the $\mathbf{MA_{C10}}$ solutions (1.01 μM; below CAC) with various concentrations of $CaCl_2$ (0.01−15.0 mM) (Figure 2b). A gradual increase of the blue shift of the $\mathbf{MA_{C10}}$ assembly was observed with increasing concentration of $CaCl_2$ reflecting an increase of the internal hydrophobicity. At 1.0 mM of $CaCl_2$, nanofibers formed hundreds of nanometers to micrometers in length (Figure S1c). The results suggested that the excess amount of counterion (Ca^{2+}) promotes the formation of nanofibers below CAC. An increase of internal hydrophobicity of $\mathbf{MA_{C10}}$ assembly for other metal chloride solutions was only observed above 1.0 mM, indicating that Ca^{2+} ions induce nanofiber formation of $\mathbf{MA_{C10}}$ more effectively than the other ions (Figure 2b). Surprisingly, also Mg^{2+} ions (above 1.0 mM) induced nanofiber formation effectively. However, the high charge density Be^{2+} and Sc^{3+} as well as large ionic radii Sr^{2+} and Ba^{2+} ions showed no significant effect on nanofibers formation. Similarly, high concentration of LiCl, NaCl, and KCl showed no significant nanofiber formation.

The complementary ionic interaction between the carboxylate moieties of $\mathbf{MA_{C10}}$ and its counterions induces the aggregation of nanofibers. Dynamic light scattering (DLS) was then employed to investigate the aggregation of $\mathbf{MA_{C10}}$ nanofibers with its counterions (concentration: 0.01 mM to 15.0 mM).[66] The molar scattering intensity of $\mathbf{MA_{C10}}$ solution (1.01 mM; above CAC) gradually increased with the concentration of $CaCl_2$, indicating that aggregation of

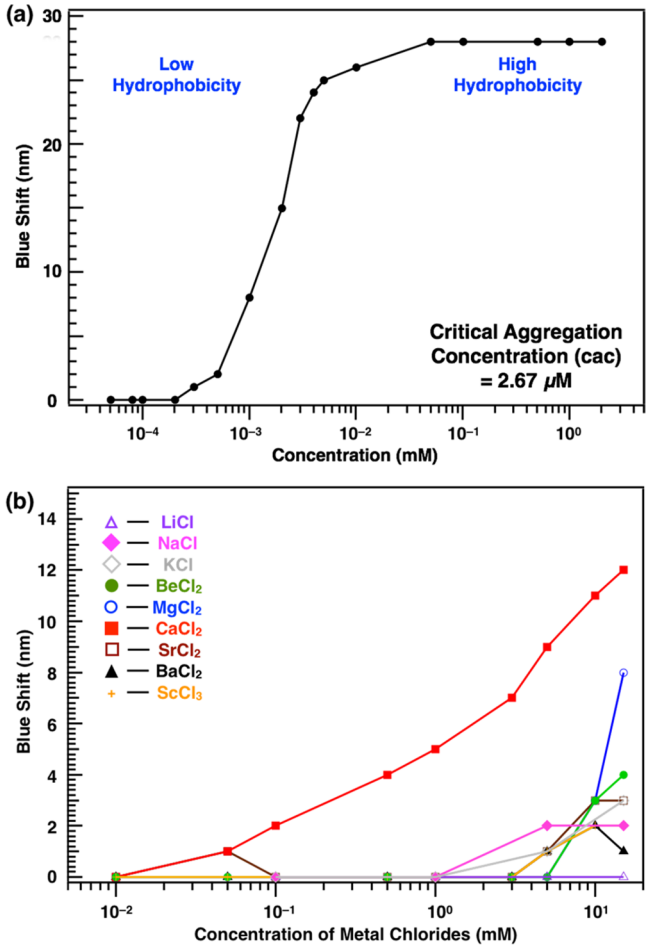

Figure 2. Nile Red fluorescence assay (a) for determination of the critical aggregation concentration of $\mathbf{MA_{C10}}$ (concentration: 5.0 × 10^{-5} to 2.0 mM) and (b) for determination of countercation effect to $\mathbf{MA_{C10}}$ (1.01 μM; below CAC) nanofiber formation concentration with various metal chlorides (concentration: 0.01−15.0 mM).

nanofibers occurred (Figure 3). At 15.0 mM of $CaCl_2$, 145.3 ± 13 M Counts s^{-1} M^{-1} molar scattering intensity was observed. A lower molar scattering intensity 45.9 ± 3 M

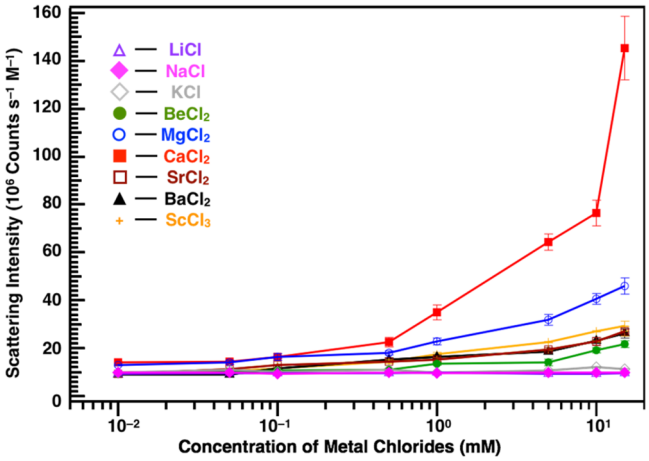

Figure 3. Molar scattering intensity of $\mathbf{MA_{C10}}$ nanofibers (1.01 mM; above CAC) in the presence of metal chlorides (concentration: 0.01 mM to 15.0 mM).

DOI: 10.1021/jacs.8b10778
J. Am. Chem. Soc. 2018, 140, 17724−17733

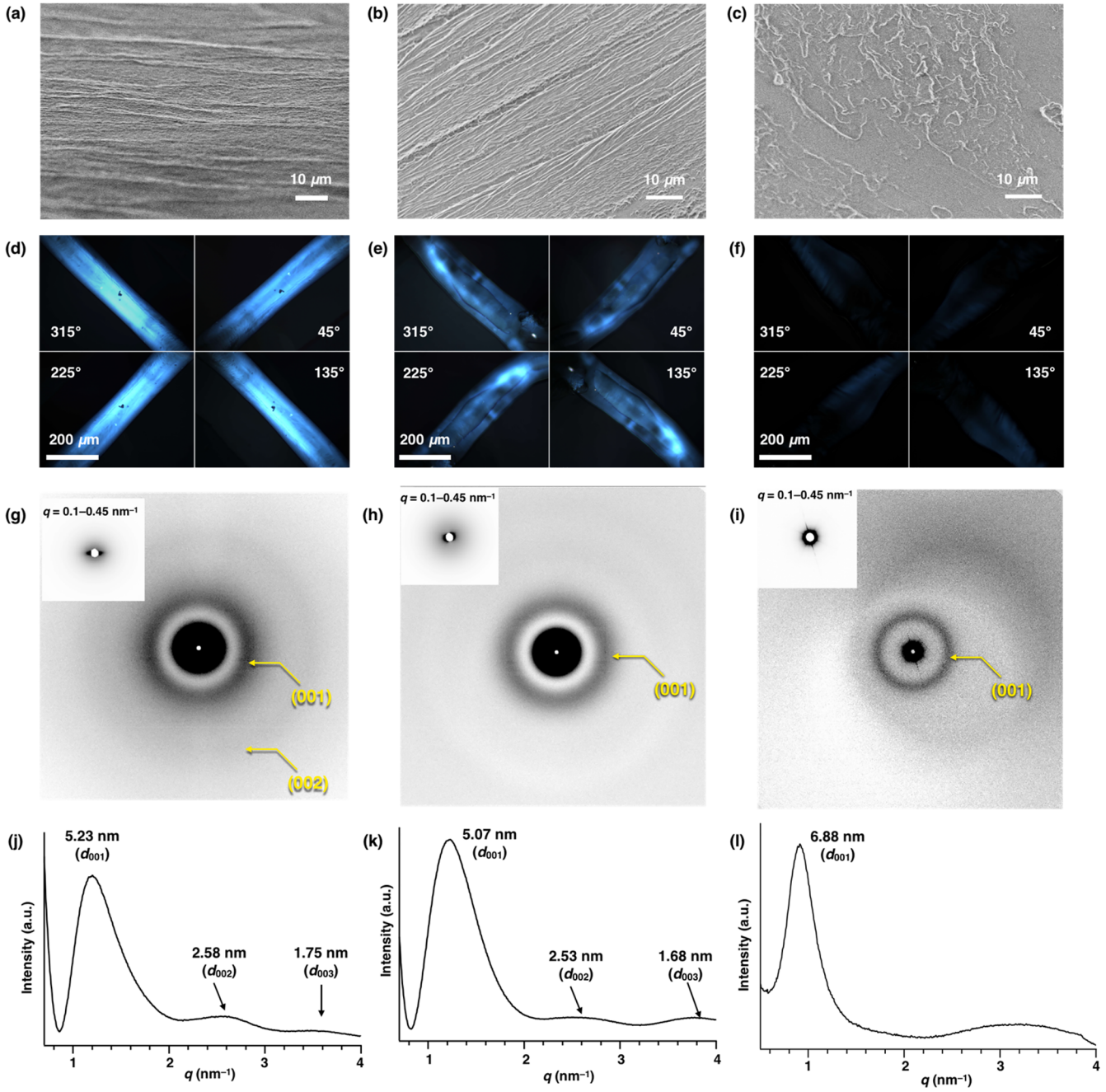

Figure 4. SEM images of a macroscopic aligned string composed of $\mathbf{MA_{C10}}$ prepared from solutions of (a) $MgCl_2$, (b) $ScCl_3$, and (c) KCl (150 mM). Optical microscopic images of a macroscopic aligned string composed of $\mathbf{MA_{C10}}$ prepared from solutions of (d) $MgCl_2$, (e) $ScCl_3$, and (f) KCl (150 mM) under crossed polarizers. The POM images of the string were tilted at 45°, 135°, 225°, and 315° relative to the transmission axis of the analyzer, the scale bar applys for all POM images. 2D SAXS images of a macroscopic aligned string composed of $\mathbf{MA_{C10}}$ prepared from solutions of (g) $MgCl_2$, (h) $ScCl_3$, and (i) KCl (150 mM) (inset: enlarged 2D image for q = 0.1−0.45 nm^{-1} at 25 °C. 1D SAXS patterns (j) $MgCl_2$, (k) $ScCl_3$, and (l) KCl of 2D SAXS images in (g) $MgCl_2$, (h) $ScCl_3$, and (i) KCl, respectively, showing the diffraction pattern in the direction perpendicular to long axis of the string.

Counts s^{-1} M^{-1} was obtained in $MgCl_2$ solutions (15.0 mM). Comparable molar scattering intensities of 26.7 ± 1 M Counts s^{-1} M^{-1}, 27.1 ± 1 M Counts s^{-1} M^{-1}, and 26.3 ± 1 M Counts s^{-1} M^{-1} were obtained in $BeCl_2$, $SrCl_2$, and $BaCl_2$ solutions (15.0 mM), respectively. Considering the binding affinity between carboxylate and M^{2+}, Ca^{2+} is expected to provide more significant aggregation.[67] However, the triple-charged Sc^{3+} (15.0 mM) afforded aggregates with a comparable molar scattering intensity 29.4 ± 2 M Counts s^{-1} M^{-1} to that of aggregates based on Be^{2+}, Sr^{2+}, and Ba^{2+} ions, possibly due to charge mismatch to $\mathbf{MA_{C10}}$ in the nanofiber structure. No significant aggregation was observed with LiCl, NaCl, and KCl adding up to 15.0 mM (Figure 3).

To further investigate the counterion effect (metal chlorides) on the interfibrillar interaction and the structure features of $\mathbf{MA_{C10}}$ nanofibers, a macroscopic string of $\mathbf{MA_{C10}}$ was prepared according to our previous reported procedure.[44] Typically, a 50.0 mM solution of $\mathbf{MA_{C10}}$ was manually drawn into an aqueous solution of $MgCl_2$ (150 mM) from a pipet, and a noodle-like string with an arbitrary length was formed.

DOI: 10.1021/jacs.8b10778
J. Am. Chem. Soc. 2018, 140, 17724−17733

Table 1. Structural Parameters and Actuation Speed of MA Strings Prepared with Metal Chlorides (M^{n+})

[a]MA/M^{n+}	d_{001} (nm)	d_{002} (nm)	d_{003} (nm)	fwhm (°)[a]	actuation speed (°/s)[b]
$\mathbf{MA_{C10}}/Be^{2+}$	4.99	–	–	124	1.02 ± 0.1
$\mathbf{MA_{C10}}/Mg^{2+}$	5.23	2.58	1.75	95	4.29 ± 0.4
$\mathbf{MA_{C10}}/Ca^{2+}$	5.48	2.70	1.82	65	7.94 ± 0.4
$\mathbf{MA_{C10}}/Sr^{2+}$	5.69	–	–	115	1.77 ± 0.3
$\mathbf{MA_{C10}}/Ba^{2+}$	5.77	–	–	isotropic	0.0
$\mathbf{MA_{C10}}/Sc^{3+}$	5.07	2.53	1.68	150	1.33 ± 0.1
$\mathbf{MA_{C10}}/Li^{+}$	6.72	–	–	isotropic	0.0
$\mathbf{MA_{C10}}/Na^{+}$	6.84	–	–	isotropic	0.0
$\mathbf{MA_{C10}}/K^{+}$	6.88	–	–	isotropic	0.0
$\mathbf{MA_{C8}}/Ca^{2+}$	5.38	–	–	110	1.84 ± 0.2
$\mathbf{MA_{C11}}/Ca^{2+}$	5.71	2.80	1.89	108	2.21 ± 0.1

[a]Full-width half-maximum (fwhm). [b]MA/M^{n+} samples prepared and photoactuation speed experiments performed, which in all cases were determined from the bending process of a string with a saturated flexion angle of 90° within a particular time, as described in the Supporting Information.

Scanning electronic microscopy (SEM) of the string, prepared from the solution of $MgCl_2$, shows arrays of unidirectionally aligned nanofiber bundles (Figure 4a), which was essentially identical to that of the string prepared from $CaCl_2$ solution (Figure S2a,b). Notably, the $\mathbf{MA_{C10}}$ strings prepared from the solutions of $BeCl_2$, $SrCl_2$, and $ScCl_3$ also showed similar morphology, that is, arrays of nanofiber bundles with unidirectional alignment, in SEM images (Figures S3a, S4a, and 4b), while no alignments were observed in the $\mathbf{MA_{C10}}$ strings prepared form solutions of $BaCl_2$, LiCl, NaCl, and KCl (Figures S5a, S6a, S7a, and 4c). The freshly prepared $\mathbf{MA_{C10}}$ string from a $MgCl_2$ solution showed uniform birefringence in the direction of the strings long axis in polarized optical microscopy (POM) images (Figures 4d and S8a), which is essentially identical to POM images of the $\mathbf{MA_{C10}}$ string obtained from $CaCl_2$ solution (Figure S2c). A lower birefringence was observed in the POM images of the $\mathbf{MA_{C10}}$ strings prepared from solutions of $BeCl_2$, $SrCl_2$, and $ScCl_3$ (Figures S3b, S4b, 4e, and S8b). In addition, no birefringence was observed in the POM images of the $\mathbf{MA_{C10}}$ strings prepared from solutions of $BaCl_2$, LiCl, NaCl, and KCl (Figures S5b, S6b, S7b, 4f, and S8c). The results indicated that $\mathbf{MA_{C10}}$ nanofibers are aligned unidirectionally in the presence of Mg^{2+} and Ca^{2+} ions, while a lower degree of alignment in $\mathbf{MA_{C10}}$ nanofibers is found in the presence of Be^{2+}, Sr^{2+}, and Sc^{3+} ions. However, no significant alignment of $\mathbf{MA_{C10}}$ nanofibers was observed in the presence of Ba^{2+}, Li^{+}, Na^{+}, and K^{+} ions.

To provide the structural parameters and orientational order, that is, degree of alignment, of the $\mathbf{MA_{C10}}$ nanofibers in the macroscopic strings, we carried out through-view small-angle X-ray scattering (SAXS) measurements. In the 2D SAXS image of the $\mathbf{MA_{C10}}$ string prepared from $MgCl_2$ solution on a sapphire substrate at 25 °C (Figure 4g), a pair of spot-like scatterings is observed in a smaller-angle region (q = 0.1−0.45 nm^{-1}) (Figure 4g, inset), which is due to scatterings from the unidirectionally aligned nanofiber bundles. The diffraction arcs with d-spacings of 5.23, 2.58, and 1.75 nm (Figure 4j), arising from the diffractions from the (001), (002), and (003) planes, respectively, of a lamellar structure, which is constructed by the unidirectionally aligned nanofibers of $\mathbf{MA_{C10}}$ with ionic interaction between Mg^{2+} and carboxylates of $\mathbf{MA_{C10}}$ as interfibrillar interaction. The layer spacing of the lamellar structure (c = 5.23 nm) of the $\mathbf{MA_{C10}}$ string prepared from $MgCl_2$ solution is shorter than that of observed $\mathbf{MA_{C10}}$ string prepared from $CaCl_2$ solution (c = 5.48 nm) (Figure S2d,e), indicating that Mg^{2+} ions induce a closer packing in the nanofibers of $\mathbf{MA_{C10}}$. The angular dependency of the peak intensity of the diffraction from the (001) plane converted from the through-view 2D SAXS image of the $\mathbf{MA_{C10}}$ string prepared from $MgCl_2$ solution (Figure 4g) showed the intensity maxima at 0° and 180° (Figure S9a). The peak intensity of the diffraction from the (001) plane was quantified by full-width half-maximum (fwhm) to obtain an ∼95° azimuthal angle, with a smaller azimuthal angle representing a larger degree of unidirectional alignment (Table 1).[68] Indeed, a smaller fwhm (∼65°) was observed in the $\mathbf{MA_{C10}}$ string prepared from $CaCl_2$ solution (Figure S9b and Table 1), indicating that a higher degree of alignment of $\mathbf{MA_{C10}}$ nanofibers is obtained in $CaCl_2$ solution.

A pair of spot-like scatterings was observed in a smaller-angle region (q = 0.1−0.45 nm^{-1}) in the 2D SAXS image of the $\mathbf{MA_{C10}}$ string prepared from solutions of $ScCl_3$, $BeCl_2$, and $SrCl_2$ (Figures 4h, S3c, and S4c, inset). The d-spacings of the diffraction arcs from the (001), (002), and (003) planes are summarized in Table 1. In accordance with the ionic radii of the cations, smaller layer spacings of a lamellar structure (c = 5.07 nm and c = 4.99 nm) were observed in the $\mathbf{MA_{C10}}$ strings prepared from solutions of $ScCl_3$ and $BeCl_2$, respectively (Figures 4k and S3d) compared to those observed with Ca^{2+} and Mg^{2+}(Table 1). Meanwhile, a larger layer spacing of a lamellar structure (c = 5.69 nm) was observed in the $\mathbf{MA_{C10}}$ strings prepared from solutions of $SrCl_2$ (Figure S4d, Table 1). In good agreement with the POM results, a lower degree of alignment was observed in the $\mathbf{MA_{C10}}$ strings prepared from solutions of $ScCl_3$, $BeCl_2$, and $SrCl_2$ (fwhm >110°, Table 1, Figure S9).

Consistent with the results obtained in SEM and POM analysis, no spot-like scatterings in a smaller-angle region (q = 0.1−0.45 nm^{-1}) and an isotropic ring of (001) diffraction plane were observed in the 2D SAXS images of the $\mathbf{MA_{C10}}$ strings prepared from solutions of $BaCl_2$, LiCl, NaCl, and KCl (Figures S5c, S6c, S7c, and 4i). The results indicated the lack of alignment of $\mathbf{MA_{C10}}$ nanofibers in the presence of Ba^{2+}, Li^{+}, Na^{+}, and K^{+} ions. On the basis of monocharged ions, larger layer spacings of lamellar structures (c = 6.72, 6.84, 6.88 nm) were observed in the $\mathbf{MA_{C10}}$ strings prepared from solutions of LiCl, NaCl, and KCl, respectively (Figures S6d, S7d, and 4l, Table 1). In accordance with the ionic radius of double-charged Ba^{2+} ion, a larger layer spacing of the lamellar structure

DOI: 10.1021/jacs.8b10778
J. Am. Chem. Soc. 2018, 140, 17724−17733

(c = 5.77 nm) was observed in the $\mathbf{MA_{C10}}$ strings prepared from solutions of $BaCl_2$ (Figure S5d, Table 1). In summary, the order for degree of unidirectional alignment in the $\mathbf{MA_{C10}}$ strings prepared form metal chloride is $Ca^{2+} > Mg^{2+} > Be^{2+} \approx Sr^{2+} \approx Sc^{3+} > Ba^{2+} \approx Li^{+} \approx Na^{+} \approx K^{+}$. A similar order of binding constants between low molecular weight organic carboxylates and alkali/alkaline earth metals has been described in the literature.[67] For instance, the binding constant of succinate-alkali/alkaline earth metal complexes follows the order $Ca^{2+} > Mg^{2+} > Sr^{2+} > Ba^{2+} > Li^{+} \approx Na^{+} \approx K^{+}$.[67] The results indicated that a higher binding constant of $\mathbf{MA_{C10}}$ and its counterions allows a structurally more ordered macroscopic string formation.

Ionic Effect of $\mathbf{MA_{C10}}$ Actuation Speed. According to the anticipated photoactuation mechanism of $\mathbf{MA_{C10}}$,[44] the photochemical isomerization of $\mathbf{MA_{C10}}$ from the stable isomer to the unstable isomer induces the actuation of the $\mathbf{MA_{C10}}$ string toward the light source(Figure 5a). With a compre-

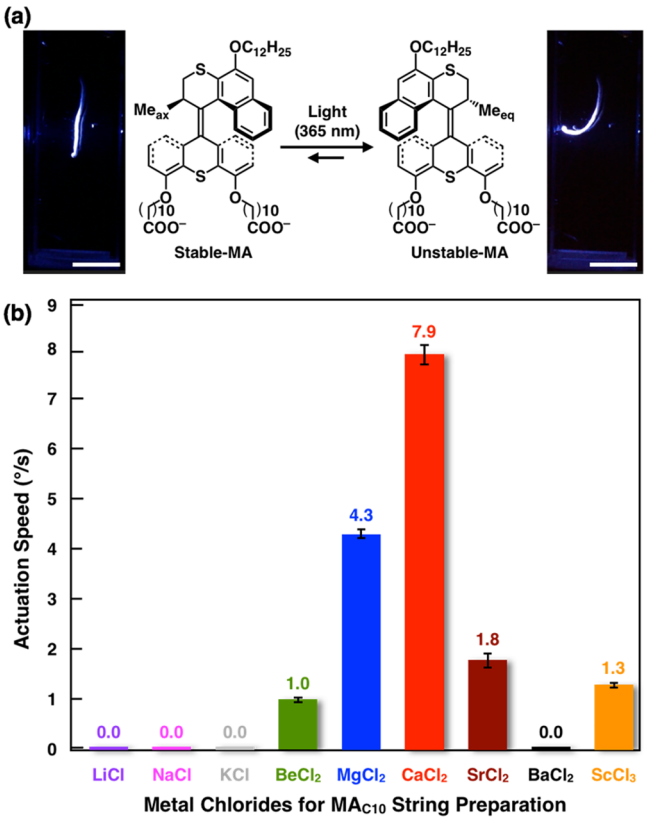

Figure 5. (a) Photoisomerization step of $\mathbf{MA_{Cn}}$ and Photoactuation of a string prepared from $\mathbf{MA_{Cn}}$ solution (50 mM), after irradiation with 365 nm light source. A single enantiomer is shown. Scale bar, 5.0 mm. (b) The actuation speed (°/s) of the $\mathbf{MA_{C10}}$ string (50.0 mM) prepared from metal chloride solutions (150 mM).

hensive structural investigation of $\mathbf{MA_{C10}}$ strings prepared from various metal chlorides solutions, the resultant hierarchical supramolecular structure, which seems to be to a large extent governed by the electrostatic interaction of M^{n+} and carboxylate groups of $\mathbf{MA_{C10}}$, would be expected to control the actuation speed of a $\mathbf{MA_{C10}}$ string. Next, a freshly prepared $\mathbf{MA_{C10}}$ string was studied in a cuvette containing an aqueous solution of $CaCl_2$ (150 mM). Upon photoirradiation (λ = 365 nm, power output 15.5 mW), the $\mathbf{MA_{C10}}$ string bent toward the light source from an initial angle of 0° to a saturated flexion angle of 90° within 15 s, indicating that the actuation speed is 7.94 ± 0.4°/s (Figure 5a,b). It should be noted that a higher power output was employed (0.7 A applied current) than in our previous study (0.2 A applied current, actuation speed = 1.5°/s),[44] providing a wider measuring window of actuation speed investigation. The $\mathbf{MA_{C10}}$ string, prepared from $MgCl_2$ solution (150 mM), bent with a saturated flexion angle of 90° within 25 s (4.29 ± 0.2°/s). Based on the degree of alignment of $\mathbf{MA_{C10}}$ strings prepared from solutions of $CaCl_2$ and $MgCl_2$ (Table 1), consistently, a higher degree of alignment of $\mathbf{MA_{C10}}$ strings provided a faster actuation toward the light source. Meanwhile, a comparable degree of alignment in the $\mathbf{MA_{C10}}$ strings prepared from solutions of $ScCl_3$, $BeCl_2$, and $SrCl_2$, showed a similar photoactuation speed (1.0−1.8°/s, Figure 5b and Table 1). In addition, the $\mathbf{MA_{C10}}$ strings prepared from solutions of $BaCl_2$, LiCl, NaCl, and KCl revealed no alignment, and no actuation was observed upon photoirradiation (Figure 5b and Table 1). In general, by choosing a particular metal chloride to prepare the $\mathbf{MA_{C10}}$ string, control over the degree of alignment of the $\mathbf{MA_{C10}}$ string and its structural packing was achieved to provide a means to control the actuation speed.

Chain Length Effect of MA Structure and its Actuation. To further elucidate key structural parameters, subsequently self-assembled structures based on motor amphiphiles with different chain length, that is, $\mathbf{MA_{C6}}$, $\mathbf{MA_{C8}}$, and $\mathbf{MA_{C11}}$, and their actuation speed were studied. The photochemical isomerization steps of $\mathbf{MA_{C6}}$, $\mathbf{MA_{C8}}$, and $\mathbf{MA_{C11}}$ were examined by ^{1}H NMR and UV−vis spectroscopy (Figures S10 and S11). Essentially identical ^{1}H NMR signal shifts were observed in CD_2Cl_2 solutions of $\mathbf{MA_{C6}}$, $\mathbf{MA_{C8}}$, and $\mathbf{MA_{C11}}$ (Figure S10),[44] and upon extended irradiation time, photostationary states with an unstable/stable isomer ratios of 9:1 were formed in CD_2Cl_2 solutions of $\mathbf{MA_{C6}}$, $\mathbf{MA_{C8}}$, and $\mathbf{MA_{C11}}$. In UV−vis absorption studies of CH_2Cl_2 solutions of $\mathbf{MA_{C6}}$, $\mathbf{MA_{C8}}$, and $\mathbf{MA_{C11}}$, an isosbestic point at 327 nm over the course of irradiation indicated that a comparable and selective photoisomerization process occurs (Figure S11). In accordance with the sample preparation method as for $\mathbf{MA_{C10}}$ (*vide supra*), freshly prepared aqueous solutions of $\mathbf{MA_{C6}}$, $\mathbf{MA_{C8}}$, and $\mathbf{MA_{C11}}$ with 2.0 equiv of NaOH were heated at 80 °C for 30 min and cooled down to room temperature to afford colorless transparent solutions, showing that the deprotonated form is soluble up to 50.0 mM concentration. Nanofibers of $\mathbf{MA_{C6}}$, $\mathbf{MA_{C8}}$, and $\mathbf{MA_{C11}}$ (1.0 mM) were observed by cryo-TEM with uniform diameter (∼5−6 nm) and several micrometers in length (Figure S12). To provide robust and stable macroscopic MA strings, 50.0 mM solutions of $\mathbf{MA_{C8}}$ or $\mathbf{MA_{C11}}$ were manually drawn into an aqueous solution of $CaCl_2$ (150 mM) from a pipet, and a noodle-like string with an arbitrary length formed, but no aligned string was formed from the solution of $\mathbf{MA_{C6}}$, possibly due to an unstable macroscopic structure formed upon addition of $CaCl_2$ (Figure S13). SEM images of the $\mathbf{MA_{C8}}$ and $\mathbf{MA_{C11}}$ strings prepared from the solution of $CaCl_2$, showed arrays of unidirectionally aligned nanofiber bundles, (Figure 6a,b), which are essentially identical to that of the $\mathbf{MA_{C10}}$ string (Figure S2a). The freshly prepared $\mathbf{MA_{C8}}$ and $\mathbf{MA_{C11}}$ strings showed a lower birefringence in the direction of their long axis in POM images (Figures 6c,d and S14) compared to that of observed in the $\mathbf{MA_{C10}}$ string (Figure S2c). The structural parameters and degree of alignment of the $\mathbf{MA_{C8}}$ and $\mathbf{MA_{C11}}$ nanofibers in the macroscopic string were again analyzed by SAXS measurement. The 2D image of the $\mathbf{MA_{C8}}$ string prepared from $CaCl_2$ solution on a sapphire

DOI: 10.1021/jacs.8b10778
J. Am. Chem. Soc. 2018, 140, 17724−17733

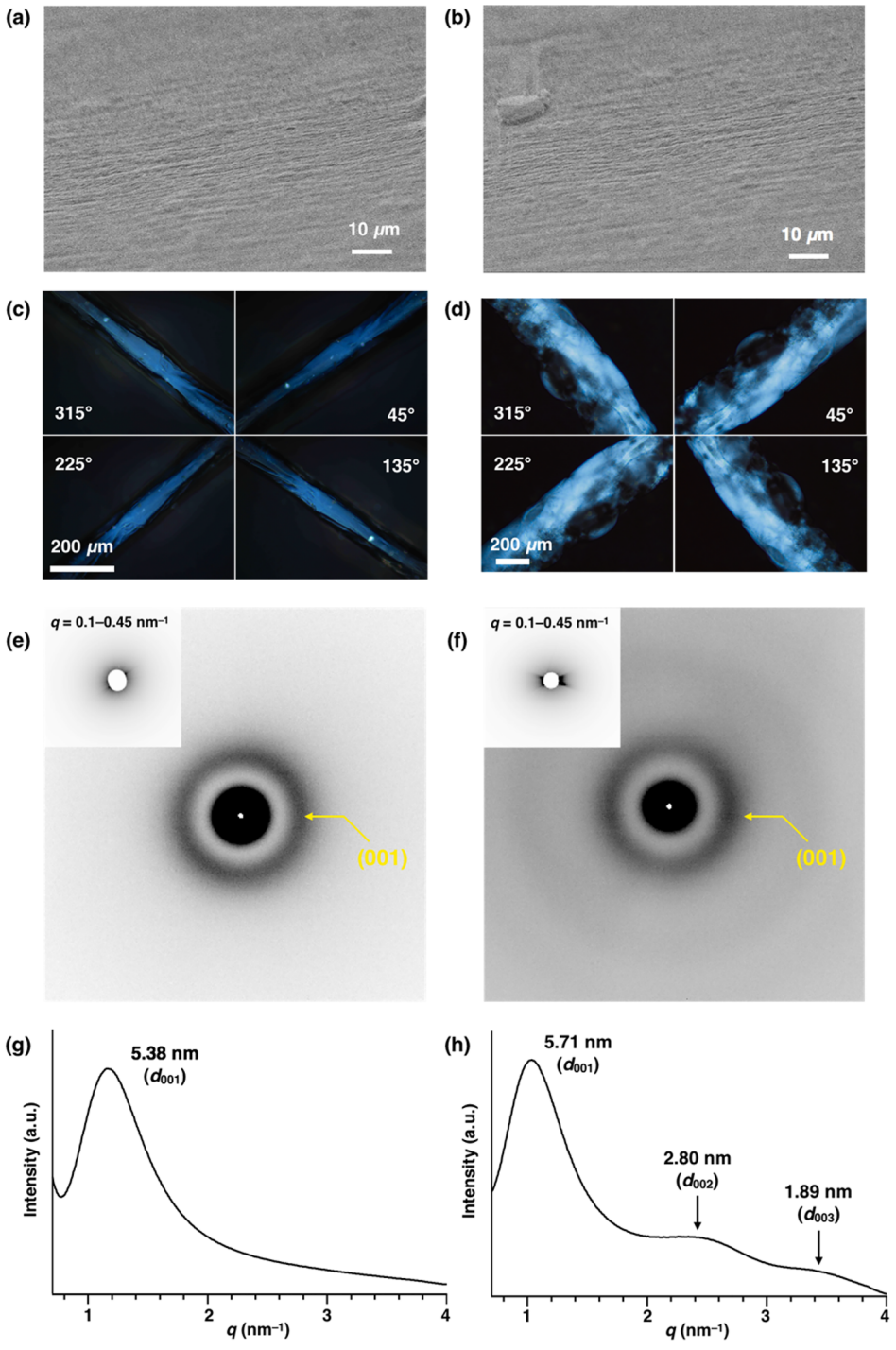

Figure 6. SEM images of a macroscopic aligned string composed of (a) $\mathbf{MA}_{\mathbf{C8}}$ and (b) $\mathbf{MA}_{\mathbf{C11}}$ prepared from an aq. $CaCl_2$ solution (150 mM). Optical microscopic images of a macroscopic aligned string composed of (c) $\mathbf{MA}_{\mathbf{C8}}$ and (d) $\mathbf{MA}_{\mathbf{C11}}$ prepared from a solution of $CaCl_2$ (150 mM) under crossed polarizers. The POM images of the string are tilted at 45°, 135°, 225°, and 315° relative to the transmission axis of the analyzer, the scale bar applys for all POM images. 2D SAXS images of a macroscopic aligned string composed of (e) $\mathbf{MA}_{\mathbf{C8}}$ and (f) $\mathbf{MA}_{\mathbf{C11}}$ prepared from a aq. solution of $CaCl_2$ (150 mM) (inset: enlarged 2D image for q = 0.1−0.45 nm^{-1} at 25 °C. 1D SAXS patterns (g) $\mathbf{MA}_{\mathbf{C8}}$ and (h) $\mathbf{MA}_{\mathbf{C11}}$ of 2D SAXS images in (e) $\mathbf{MA}_{\mathbf{C8}}$ and (f) $\mathbf{MA}_{\mathbf{C11}}$, respectively, showing the diffraction pattern in the direction perpendicular to long axis of the string.

substrate at 25 °C (Figure 6e,f) revealed a weak pair of spot-like scatterings in a smaller-angle region (q = 0.1−0.45 nm^{-1}) (Figure 6e, inset), and the diffraction arc of the (001) plane with d-spacing of 5.38 nm of a lamellar structure was observed (Figure 6g). Higher order diffraction planes (002) and (003) were found in the $\mathbf{MA}_{\mathbf{C11}}$ string prepared from a $CaCl_2$ solution (Figure 6f,h). The layer spacing of the lamellar structure (c = 5.38 nm) of the $\mathbf{MA}_{\mathbf{C8}}$ is shorter than that of the $\mathbf{MA}_{\mathbf{C10}}$ string (c = 5.48 nm) (Figure S2e) and $\mathbf{MA}_{\mathbf{C11}}$ string (c = 5.71 nm), indicating that the shorter alkyl-linker in **MA** induces a closer packing of the **MA** nanofibers in the corresponding macroscopic string. In good agreement with POM results, lower degrees of alignments were observed in the $\mathbf{MA}_{\mathbf{C8}}$ (fwhm = 110°) and $\mathbf{MA}_{\mathbf{C11}}$ (fwhm = 108°) strings

DOI: 10.1021/jacs.8b10778
J. Am. Chem. Soc. 2018, 140, 17724−17733

(Table 1, Figure S9). Upon photoirradiation, the freshly prepared $\mathbf{MA}_{C8}$ and $\mathbf{MA}_{C11}$ strings bent toward the light source from an initial angle of 0° to a saturated flexion angle of 90° with an actuation speed of 1.84 ± 0.2°/s and 2.21 ± 0.1°/s, respectively, which were slower than that seen for the $\mathbf{MA}_{C10}$ string prepared in the aqueous $CaCl_2$ solution (Table 1). These results clearly demonstrate that the structure of motor amphiphile is crucial to the macroscopic responsive behavior and there is a distinct effect of chain length going from $n = 6$ (no actuation) to $n = 11$ (slower actuation).

CONCLUSION

Motor amphiphiles with various chain lengths at the lower half of the motor moiety were synthesized and probed for their self-assembly properties. Nanofibers of $\mathbf{MA}_{C6}$, $\mathbf{MA}_{C8}$, $\mathbf{MA}_{C10}$, and $\mathbf{MA}_{C11}$ in water were observed by cryo-TEM. As shown by NRFA, calcium ions enhanced the formation nanofibers of $\mathbf{MA}_{C10}$ dramatically, while other ions were shown less effective. DLS measurements were consistent with NRFS showing that the calcium-ion-induced nanofiber aggregation of $\mathbf{MA}_{C10}$ is more efficient than with the other ions used in present study. By applying a shear flow method, macroscopic strings of $\mathbf{MA}_{C10}$ prepared in the presence of calcium and magnesium ions provided a higher degree of alignment which facilitated a faster response to light during photoactuation. The current approach demonstrates the potential of generating muscle-like functions with distinct mobility, allowing access to multiple photoresponsive supramolecular actuation systems from identical molecular structure. We envisage that a permanent macroscopic motion powered by light might be feasible by employing a molecular motor with a lower barrier for the thermal helix inversion step, and studies toward such systems are currently in progress.

ASSOCIATED CONTENT

Supporting Information

The Supporting Information is available free of charge on the ACS Publications website at DOI: 10.1021/jacs.8b10778.

Synthesis, ^1H and ^{13}C NMR spectra, UV−vis spectra, POM images, XRD profiles, XRD images, SEM images, cryo-TEM images (PDF)

AUTHOR INFORMATION

Corresponding Author

*b.l.feringa@rug.nl

ORCID

Franco King-Chi Leung: 0000-0003-0895-9307
Jiawen Chen: 0000-0002-0251-8976
Marc C. A. Stuart: 0000-0003-0667-6338
Takanori Fukushima: 0000-0001-5586-9238
Ben L. Feringa: 0000-0003-0588-8435

Notes

The authors declare no competing financial interest.

ACKNOWLEDGMENTS

This work was supported financially by the Croucher Foundation (Croucher Postdoctoral Fellowship to F.K.C.L.), The Netherlands Organization for Scientific Research (NWO−CW), the European Research Council (ERC; advanced grant no. 694345 to B.L.F.), the Ministry of Education, Culture and Science (Gravitation program no. 024.001.035), and a Grant-in-Aid for Scientific Research on Innovative Areas "π-Figuration" (nos. 26102008 and 15K21721) of The Ministry of Education, Culture, Sports, Science and Technology (MEXT), Japan. The synchrotron XRD experiments were performed at the BL45XU in the SPring-8 with the approval of the RIKEN SPring-8 Center (proposal no. 20160027). Part of work has been performed at the Giepmans lab, which is sponsored by ZonMW grant 91111.006 (ATLAS); NMW 175-010-2009-023 (Zeiss confocal) and STW Microscopy Valley 12718 (CLEM).

REFERENCES

(1) Fletcher, D. A.; Mullins, R. D. Cell Mechanics and the Cytoskeleton. *Nature* **2010**, *463*, 485−492.
(2) Huber, F.; Schnauß, J.; Rönicke, S.; Rauch, P.; Müller, K.; Fütterer, C.; Käs, J. Emergent Complexity of the Cytoskeleton: From Single Filaments to Tissue. *Adv. Phys.* **2013**, *62*, 1−112.
(3) Lino, T. Assembly of Salmonella Flagellin in Vitro and in Vivo. *J. Supramol. Struct.* **1974**, *2*, 372−384.
(4) Simmons, N. S.; Blout, E. R. The Structure of Tobacco Mosaic Virus and Its Components: Ultraviolet Optical Rotatory Dispersion. *Biophys. J.* **1960**, *1*, 55−62.
(5) Lehn, J. M. Supramolecular Polymer Chemistry - Scope and Perspective. *Polym. Int.* **2002**, *51* (10), 825−839.
(6) Wojtecki, R. J.; Meador, M. A.; Rowan, S. J. Using the Dynamic Bond to Access Macroscopically Responsive Structurally Dynamic Polymers. *Nat. Mater.* **2011**, *10*, 14−27.
(7) Yan, X.; Wang, F.; Zheng, B.; Huang, F. Stimuli-Responsive Supramolecular Polymeric Materials. *Chem. Soc. Rev.* **2012**, *41*, 6042−6065.
(8) Dong, R.; Zhou, Y.; Huang, X.; Zhu, X.; Lu, Y.; Shen, J. Functional Supramolecular Polymers for Biomedical Applications. *Adv. Mater.* **2015**, *27*, 498−526.
(9) de Greef, T. F. A.; Meijer, E. W. Supramolecular Polymers. *Nature* **2008**, *453*, 171−173.
(10) Krieg, E.; Rybtchinski, B. Noncovalent Water-Based Materials: Robust yet Adaptive. *Chem. - Eur. J.* **2011**, *17*, 9016−9026.
(11) Li, S. L.; Xiao, T.; Lin, C.; Wang, L. Advanced Supramolecular Polymers Constructed by Orthogonal Self-Assembly. *Chem. Soc. Rev.* **2012**, *41*, 5950−5968.
(12) Aida, T.; Meijer, E. W.; Stupp, S. I. Functional Supramolecular Polymers. *Science* **2012**, *335*, 813−817.
(13) Palmer, L. C.; Stupp, S. I. Molecular Self-Assembly into One-Dimensional Nanostructures. *Acc. Chem. Res.* **2008**, *41*, 1674−1684.
(14) Oshovsky, G. V.; Reinhoudt, D. N.; Verboom, W. Supramolecular Chemistry in Water. *Angew. Chem., Int. Ed.* **2007**, *46*, 2366−2393.
(15) Mulder, A.; Huskens, J.; Reinhoudt, D. N. Multivalency in Supramolecular Chemistry and Nanofabrication. *Org. Biomol. Chem.* **2004**, *2*, 3409−3424.
(16) Hamley, I. W. Self-Assembly of Amphiphilic Peptides. *Soft Matter* **2011**, *7*, 4122−4138.
(17) Smith, K. H.; Tejeda-Montes, E.; Poch, M.; Mata, A. Integrating Top-down and Self-Assembly in the Fabrication of Peptide and Protein-Based Biomedical Materials. *Chem. Soc. Rev.* **2011**, *40*, 4563−4577.
(18) (a) Yang, S. K.; Zimmerman, S. C. Hydrogen Bonding Modules for Use in Supramolecular Polymers. *Isr. J. Chem.* **2013**, *53*, 511−520. (b) Cantekin, S.; de Greef, T. F. A.; Palmans, A. R. A. Benzene-1,3,5-Tricarboxamide: A Versatile Ordering Moiety for Supramolecular Chemistry. *Chem. Soc. Rev.* **2012**, *41*, 6125−6137.
(19) Dankers, P. Y. W.; Hermans, T. M.; Baughman, T. W.; Kamikawa, Y.; Kieltyka, R. E.; Bastings, M. M. C.; Janssen, H. M.; Sommerdijk, N. A. J. M.; Larsen, A.; van Luyn, M. J. A.; Bosman, A. W.; Popa, E. R.; Fytas, G.; Meijer, E. W. Hierarchical Formation of Supramolecular Transient Networks in Water: A Modular Injectable Delivery System. *Adv. Mater.* **2012**, *24*, 2703−2709.

DOI: 10.1021/jacs.8b10778
J. Am. Chem. Soc. 2018, 140, 17724−17733

(20) Sijbesma, R. P.; Beijer, F. H.; Brunsveld, L.; Folmer, B. J. B.; Hirschberg, J. H. K. K.; Lange, R. F. M.; Lowe, J. K. L.; Meijer, E. W. Reversible Polymers Formed from Self-Complementary Monomers Using Quadruple Hydrogen Bonding. *Science* **1997**, *278*, 1601−1604.
(21) Hirschberg, J. H. K. K.; Brunsveld, L.; Ramzi, A.; Vekemans, J. A. J. M.; Sijbesma, R. P.; Meijer, E. W. Helical Self-Assembled Polymers from Cooperative Stacking of Hydrogen-Bonded Pairs. *Nature* **2000**, *407*, 167−170.
(22) Fenniri, H.; Mathivanan, P.; Vidale, K. L.; Sherman, D. M.; Hallenga, K.; Wood, K. V.; Stowell, J. G. Helical Rosette Nanotubes: Design, Self-Assembly, and Characterization. *J. Am. Chem. Soc.* **2001**, *123*, 3854−3855.
(23) Johnson, R. S.; Yamazaki, T.; Kovalenko, A.; Fenniri, H. Molecular Basis for Water-Promoted Supramolecular Chirality Inversion in Helical Rosette Nanotubes. *J. Am. Chem. Soc.* **2007**, *129* (17), 5735−5743.
(24) Maity, C.; Hendriksen, W. E.; van Esch, J. H.; Eelkema, R. Spatial Structuring of a Supramolecular Hydrogel by Using a Visible-Light Triggered Catalyst. *Angew. Chem., Int. Ed.* **2015**, *54*, 998−1001.
(25) Chebotareva, N.; Bomans, P. H. H.; Frederik, P. M.; Sommerdijk, N. A. J. M.; Sijbesma, R. P. Morphological Control and Molecular Recognition by Bis-Urea Hydrogen Bonding in Micelles of Amphiphilic Tri-Block Copolymers. *Chem. Commun.* **2005**, 4967−4969.
(26) Tidhar, Y.; Weissman, H.; Wolf, S. G.; Gulino, A.; Rybtchinski, B. Pathway-Dependent Self-Assembly of Perylene Diimide/Peptide Conjugates in Aqueous Medium. *Chem. - Eur. J.* **2011**, *17*, 6068−6075.
(27) Würthner, F. Perylene Bisimide Dyes as Versatile Building Blocks for Functional Supramolecular Architectures. *Chem. Commun.* **2004**, *4*, 1564−1579.
(28) Golubkov, G.; Weissman, H.; Shirman, E.; Wolf, S. G.; Pinkas, I.; Rybtchinski, B. Economical Design in Noncovalent Nanoscale Synthesis: Diverse Photofunctional Nanostructures Based on a Single Covalent Building Block. *Angew. Chem., Int. Ed.* **2009**, *48*, 926−930.
(29) Lee, D. W.; Kim, T.; Park, I. S.; Huang, Z.; Lee, M. Multivalent Nanofibers of a Controlled Length: Regulation of Bacterial Cell Agglutination. *J. Am. Chem. Soc.* **2012**, *134*, 14722−14725.
(30) Shin, S.; Lim, S.; Kim, Y.; Kim, T.; Choi, T. L.; Lee, M. Supramolecular Switching between Flat Sheets and Helical Tubules Triggered by Coordination Interaction. *J. Am. Chem. Soc.* **2013**, *135*, 2156−2159.
(31) Görl, D.; Zhang, X.; Stepanenko, V.; Würthner, F. Supramolecular Block Copolymers by Kinetically Controlled Co-Self-Assembly of Planar and Core-Twisted Perylene Bisimides. *Nat. Commun.* **2015**, *6*, 7009.
(32) Weingarten, A. S.; Kazantsev, R. V.; Palmer, L. C.; McClendon, M.; Koltonow, A. R.; Samuel, A. P. S.; Kiebala, D. J.; Wasielewski, M. R.; Stupp, S. I. Self-Assembling Hydrogel Scaffolds for Photocatalytic Hydrogen Production. *Nat. Chem.* **2014**, *6*, 964−970.
(33) Zhang, G.; Jin, W.; Fukushima, T.; Kosaka, A.; Ishii, N.; Aida, T. Formation of Water-Dispersible Nanotubular Graphitic Assembly Decorated with Isothiouronium Ion Groups and Its Supramolecular Functionalization. *J. Am. Chem. Soc.* **2007**, *129* (3), 719−722.
(34) Zhang, S.; Greenfield, M. A.; Mata, A.; Palmer, L. C.; Bitton, R.; Mantei, J. R.; Aparicio, C.; Olvera de la Cruz, M.; Stupp, S. I. A Self-Assembly Pathway to Aligned Monodomain Gels. *Nat. Mater.* **2010**, *9*, 594−601.
(35) Wang, C.; Guo, Y.; Wang, Y.; Xu, H.; Wang, R.; Zhang, X. Supramolecular Amphiphiles Based on a Water-Soluble Charge Transfer Complex: Fabrication of Ultralong Nanofibers with Tunable Straightness. *Angew. Chem., Int. Ed.* **2009**, *48*, 8962−8965.
(36) Brizard, A.; Aimé, C.; Labrot, T.; Huc, I.; Berthier, D.; Artzner, F.; Desbat, B.; Oda, R. Counterion, Temperature, and Time Modulation of Nanometric Chiral Ribbons from Gemini-Tartrate Amphiphiles. *J. Am. Chem. Soc.* **2007**, *129*, 3754−3762.
(37) Wu, Z. L.; Kurokawa, T.; Liang, S.; Furukawa, H.; Gong, J. P. Hydrogels with Cylindrically Symmetric Structure at Macroscopic Scale by Self-Assembly of Semi-Rigid Polyion Complex. *J. Am. Chem. Soc.* **2010**, *132*, 10064−10069.
(38) Matson, J. B.; Stupp, S. I. Self-Assembling Peptide Scaffolds for Regenerative Medicine. *Chem. Commun.* **2012**, *48*, 26−33.
(39) Stupp, S. I.; Zha, R. H.; Palmer, L. C.; Cui, H.; Bitton, R. Self-Assembly of Biomolecular Soft Matter. *Faraday Discuss.* **2013**, *166*, 9−30.
(40) Webber, M. J.; Berns, E. J.; Stupp, S. I. Supramolecular Nanofibers of Peptide Amphiphiles for Medicine. *Isr. J. Chem.* **2013**, *53*, 530−554.
(41) Wall, B. D.; Diegelmann, S. R.; Zhang, S.; Dawidczyk, T. J.; Wilson, W. L.; Katz, H. E.; Mao, H. Q.; Tovar, J. D. Aligned Macroscopic Domains of Optoelectronic Nanostructures Prepared via Shear-Flow Assembly of Peptide Hydrogels. *Adv. Mater.* **2011**, *23*, 5009−5014.
(42) Sanders, A. M.; Magnanelli, T. J.; Bragg, A. E.; Tovar, J. D. Photoinduced Electron Transfer within Supramolecular Donor-Acceptor Peptide Nanostructures under Aqueous Conditions. *J. Am. Chem. Soc.* **2016**, *138*, 3362−3370.
(43) Besar, K.; Ardoña, H. A. M.; Tovar, J. D.; Katz, H. E. Demonstration of Hole Transport and Voltage Equilibration in Self-Assembled π-Conjugated Peptide Nanostructures Using Field-Effect Transistor Architectures. *ACS Nano* **2015**, *9*, 12401−12409.
(44) Chen, J.; Leung, F. K. C.; Stuart, M. C. A.; Kajitani, T.; Fukushima, T.; van der Giessen, E.; Feringa, B. L. Artificial Muscle-like Function from Hierarchical Supramolecular Assembly of Photoresponsive Molecular Motors. *Nat. Chem.* **2018**, *10*, 132−138.
(45) Irie, M.; Fukaminato, T.; Matsuda, K.; Kobatake, S. Photochromism of Diarylethene Molecules and Crystals : Memories, Switches, and Actuators. *Chem. Rev.* **2014**, *114*, 12174−12277.
(46) Ikegami, T.; Kageyama, Y.; Obara, K.; Takeda, S. Dissipative and Autonomous Square-Wave Self-Oscillation of a Macroscopic Hybrid Self-Assembly under Continuous Light Irradiation. *Angew. Chem., Int. Ed.* **2016**, *55*, 8239−8243.
(47) Morimoto, M.; Irie, M. A Diarylethene Cocrystal That Converts Light into Mechanical Work. *J. Am. Chem. Soc.* **2010**, *132*, 14172−14178.
(48) Kitagawa, D.; Nishi, H.; Kobatake, S. Photoinduced Twisting of a Photochromic Diarylethene Crystal. *Angew. Chem., Int. Ed.* **2013**, *52*, 9320−9322.
(49) Harada, A.; Takashima, Y.; Nakahata, M. Supramolecular Polymeric Materials via Cyclodextrin Guest Interactions. *Acc. Chem. Res.* **2014**, *47*, 2128−2140.
(50) Iwaso, K.; Takashima, Y.; Harada, A. Fast Response Dry-Type Artificial Molecular Muscles with [C2] Daisy Chains. *Nat. Chem.* **2016**, *8*, 625−632.
(51) Li, Q.; Fuks, G.; Moulin, E.; Maaloum, M.; Rawiso, M.; Kulic, I.; Foy, J. T.; Giuseppone, N. Macroscopic Contraction of a Gel Induced by the Integrated Motion of Light-Driven Molecular Motors. *Nat. Nanotechnol.* **2015**, *10*, 161−165.
(52) Foy, J. T.; Li, Q.; Goujon, A.; Colard-Itté, J.-R.; Fuks, G.; Moulin, E.; Schiffmann, O.; Dattler, D.; Funeriu, D. P.; Giuseppone, N. Dual-Light Control of Nanomachines That Integrate Motor and Modulator Subunits. *Nat. Nanotechnol.* **2017**, *12*, 540−545.
(53) Ikeda, T.; Mamiya, J.; Yu, Y. Artificial Muscles Photomechanics of Liquid-Crystalline Elastomers and Other Polymers. *Angew. Chem., Int. Ed.* **2007**, *46*, 506−528.
(54) White, T. J.; Broer, D. J. Programmable and Adaptive Mechanics with Liquid Crystal Polymer Networks and Elastomers. *Nat. Mater.* **2015**, *14*, 1087−1098.
(55) Aßhoff, S. J.; Lancia, F.; Iamsaard, S.; Matt, B.; Kudernac, T.; Fletcher, S. P.; Katsonis, N. High-Power Actuation from Molecular Photoswitches in Enantiomerically Paired Soft Springs. *Angew. Chem., Int. Ed.* **2017**, *56*, 3261−3265.
(56) Gelebart, A. H.; Mulder, D. J.; Varga, M.; Konya, A.; Vantomme, G.; et al. Making Waves in a Photoactive Polymer Film. *Nature* **2017**, *546*, 632−636.

DOI: 10.1021/jacs.8b10778
J. Am. Chem. Soc. 2018, 140, 17724−17733

(57) Iamsaard, S.; Aßhoff, S. J.; Matt, B.; Kudernac, T.; Cornelissen, J. J. L. M.; Fletcher, S. P.; Katsonis, N. Conversion of Light into Macroscopic Helical Motion. *Nat. Chem.* **2014**, *6*, 229−235.
(58) Camacho-lopez, M.; Finkelmann, H.; Palffy-muhoray, P.; Shelley, M. Fast Liquid-Crystal Elastomer Swims into the Dark. *Nat. Mater.* **2004**, *3*, 307−310.
(59) van Oosten, C. L.; Bastiaansen, C. W. M.; Broer, D. J. Printed Artificial Cilia from Liquid-Crystal Network Actuators Modularly Driven by Light. *Nat. Mater.* **2009**, *8*, 677−682.
(60) Greenfield, M. A.; Hoffman, J. R.; Olvera de la Cruz, M.; Stupp, S. I. Tunable Mechanics of Peptide Nanofiber Gels. *Langmuir* **2010**, *26*, 3641−3647.
(61) Chen, L.; Pont, G.; Morris, K.; Lotze, G.; Squires, A.; Serpell, L. C.; Adams, D. J. Salt-Induced Hydrogelation of Functionalised-Dipeptides at High pH. *Chem. Commun.* **2011**, *47*, 12071−12073.
(62) Chin, S. M.; Synatschke, C. V.; Liu, S.; Nap, R. J.; Sather, N. A.; Wang, Q.; Álvarez, Z.; Edelbrock, A. N.; Fyrner, T.; Palmer, L. C.; Szleifer, I.; Olvera de la Cruz, M.; Stupp, S. I. Covalent-Supramolecular Hybrid Polymers as Muscle-Inspired Anisotropic Actuators. *Nat. Commun.* **2018**, *9*, 2395.
(63) Georges, P. C.; Miller, W. J.; Meaney, D. F.; Sawyer, E. S.; Janmey, P. A. Matrices with Compliance Comparable to That of Brain Tissue Select Neuronal over Glial Growth in Mixed Cortical Cultures. *Biophys. J.* **2006**, *90*, 3012−3018.
(64) Georges, P. C.; Janmey, P. A. Cell Type-Specific Response to Growth on Soft Materials. *J. Appl. Physiol.* **2005**, *98*, 1547−1553.
(65) Wang, H.-B.; Dembo, M.; Wang, Y.-L. Substrate Flexibility Regulates Growth and Apoptosis of Normal but Not Transformed Cells. *Am. J. Physiol. Physiol.* **2000**, *279*, 1345−1350.
(66) Tantakitti, F.; Boekhoven, J.; Wang, X.; Kazantsev, R. V.; Yu, T.; Li, J.; Zhuang, E.; Zandi, R.; Ortony, J. H.; Newcomb, C. J.; Palmer, L. C.; Shekhawat, G. S.; Olvera de la Cruz, M.; Schatz, G. C.; Stupp, S. I. Energy Landscapes and Functions of Supramolecular Systems. *Nat. Mater.* **2016**, *15*, 469−476.
(67) (a) Dudev, T.; Lim, C. Monodentate versus Bidentate Carboxylate Binding in Magnesium and Calcium Proteins: What Are the Basic Principles. *J. Phys. Chem. B* **2004**, *108*, 4546−4557. (b) Daniele, P. G.; Foti, C.; Gianguzza, A.; Prenesti, E.; Sammartano, S. Weak Alkali and Alkaline Earth Metal Complexes of Low Molecular Weight Ligands in Aqueous Solution. *Coord. Chem. Rev.* **2008**, *252*, 1093−1107. (c) de Robertis, A.; de Stefano, C.; Scarcella, R.; Rigano, C. Thermodynamic of Formation of Magnesium(II), Calcium(II), Strontium(II) and Barium(II)-Succinate Complexes in Aqueous Solution. *Thermochim. Acta* **1984**, *80*, 197−208.
(68) Siqueira, G.; Kokkinis, D.; Libanori, R.; Hausmann, M. K.; Gladman, A. S.; Neels, A.; Tingaut, P.; Zimmermann, T.; Lewis, J. A.; Studart, A. R. Cellulose Nanocrystal Inks for 3D Printing of Textured Cellular Architectures. *Adv. Funct. Mater.* **2017**, *27*, 1604619.

DOI: 10.1021/jacs.8b10778
J. Am. Chem. Soc. 2018, 140, 17724−17733